Meteorol. Z. (Contrib. Atm. Sci.), Vol. **29**, No. 6, 501–509 (published online September 4, 2020)

Short Contributions

Balloon-borne radiation measurements demonstrate radiative forcing by water vapor and clouds

Rolf Philipona[1*], Andreas Kräuchi[2], Rigel Kivi[3], Thomas Peter[2], Martin Wild[2], Ruud Dirksen[4], Masatomo Fujiwara[5], Miho Sekiguchi[6], Dale F. Hurst[7,8] and Ralf Becker[4]

[1]Federal Office of Meteorology and Climatology MeteoSwiss (retired), Payerne, Switzerland
[2]Institute for Atmospheric and Climate Science, ETH Zurich, Zurich, Switzerland
[3]Finnish Meteorological Institute, Sodankylä, Finland
[4]German Weather Service, Meteorological Observatory Lindenberg, Germany
[5]Faculty of Environmental Earth Science, Hokkaido University, Sapporo, Japan
[6]Tokyo University of Marine Science and Technology, Tokyo, Japan
[7]Cooperative Institute for Research in Environmental Sciences, University of Colorado, Boulder, CO, USA
[8]NOAA Earth System Research Laboratory, Global Monitoring Division, Boulder, CO, USA

(Manuscript received June 3, 2020; in revised form July 26, 2020; accepted July 27, 2020)

Abstract

Solar shortwave and terrestrial thermal longwave irradiance are measured at radiation sites at the Earth's surface and on satellite platforms high up in space, since many years. Radiation profiles through the Earth's atmosphere, however, have only sporadically been measured from enhanced upper-air radiosondes. Here we show profiles of solar and terrestrial radiation measured with balloon-borne radiometers through cloud-free and cloudy atmospheres, which reveal radiative effects of temperature, water vapor, ozone and clouds on downward and upward radiation. Shortwave radiation profiles show solar absorption in the free atmosphere and strong reflection in clouds and albedo effects on the ground and the atmosphere above. Longwave upward radiation profiles visualize terrestrial radiation emitted from the Earth's surface, which is partly absorbed and reemitted in the boundary layer and in the atmosphere by water vapor and other greenhouse gases. Longwave downward radiation profiles show the absorbed terrestrial radiation in the atmosphere and reveal the warming effect of increasing greenhouse gases, and by this visualize and demonstrate radiative forcing and a changing greenhouse effect by water vapor in the Earth's atmosphere. Longwave net radiation profiles show terrestrial emission into space to be reduced by water vapor and clouds. Measured radiation profiles are compared to numerically calculated radiation profiles.

Keywords: Solar and terrestrial radiation, Atmospheric radiation profile measurements, Radiative forcing, Greenhouse effect

1 Introduction

Climate change is a major concern for our society. Global warming is driven by anthropogenic greenhouse gases (GHGs) such as CO_2, CH_4, N_2O and others, which in addition to the natural greenhouse gases absorb and reemit terrestrial longwave radiation. Enhanced absorption of terrestrial longwave radiation by anthropogenic greenhouse gases leads to an imbalance of incoming and outgoing energy in the Earth-atmosphere system over time, which is called radiative forcing. Radiative forcing raises temperatures at the surface and in the troposphere, which leads to an increase of the concentration of the strongest greenhouse gas, water vapor, and thereby strengthens the greenhouse effect through water vapor feedback. Solar shortwave radiation on the other hand is absorbed by water vapor, and reflected by aerosols and clouds leading to positive and negative radiative forcing, respectively.

*Corresponding author: Rolf Philipona, Tschuggenstrasse 39, 7260 Davos Dorf, Switzerland, e-mail: rolf.philipona@gmail.com

Solar radiation is the main energy source of our planet and has been measured at the Earth's surface as direct and global radiation for more than a century (Fröhlich, 1991). Total solar irradiance (TSI) has been measured from space since 1979 (Willson, 1997; Fröhlich and Lean, 2004) and composite time-series are available over three solar cycles (Foukal et al., 2006; Kopp and Lean, 2011). Radiance spectra of outgoing shortwave and longwave radiation at the top of the atmosphere, measured from satellites since the late 1960s, allow for estimates of the radiation budget and investigations of the radiative forcing of climate in the Earth-atmosphere system (Raschke et al., 1973; Ramanathan et al., 1989; Trenberth et al., 2009). Terrestrial longwave radiation has been reliably measured at the Earth's surface since the 1990s (Philipona et al., 2001) and national and international radiation networks allowed to measure rising longwave downward irradiance (Philipona et al., 2004; Wild et al., 2008). Broadband and spectrally resolved shortwave downward and upward radiation was measured from airplanes primar-

DOI 10.1127/metz/2020/1044
Gebrüder Borntraeger Science Publishers, Stuttgart, www.borntraeger-cramer.com

ily in the lower troposphere to investigate aerosol- and cloud-radiation interaction and to test and improve radiative transfer calculations (Wendisch et al., 1996; Wendisch and Keil, 1999; Wendling et al., 2002; Wendisch and Mayer, 2003; Guan et al., 2010). Vertical shortwave and longwave radiation profiles through the atmosphere were only sporadically measured with simple instruments in the 1950s (Suomi et al., 1958), and later in only few experiments at diverse locations in the world (Paltridge and Sargent, 1971; Yamamoto et al., 1995; Asano et al., 2004).

Upper-air observations for climate have recently been given more attention with the initiation of the GCOS (Global Climate Observing System) Reference Upper Air Network (GRUAN) to provide reference-quality measurements of essential climate variables in the troposphere and lower stratosphere (GCOS, 2007; Seidel et al., 2009). The primary objectives of GRUAN are to monitor changes in temperature and water vapor profiles in the upper troposphere and lower stratosphere (UTLS) (Thorne et al., 2005; Randel et al., 2006; Philipona et al., 2018). The enhanced greenhouse effect of a given increase in greenhouse gases and water vapor appears to be larger in the UTLS than in the lower troposphere (Held and Soden, 2000; Hansen et al., 2005; Solomon et al., 2010). Also, high clouds particularly affect longwave emission into space (Ohring and Clapp, 1980; Eyring et al., 2005), whereas low clouds affect the planet's shortwave albedo.

We recently measured solar and terrestrial radiation profiles through cloud-free atmospheres using balloon-borne radiation instruments, and parachute and double balloon techniques for the instrument recovery (Philipona et al., 2012; Kräuchi et al., 2016). During a 2015 campaign in Sodankylä, Finland, we employed a novel Return Glider Radiosonde (RGR) to recover the radiation instruments (Kräuchi and Philipona, 2016). Here, we present the scientific evaluation of shortwave and longwave irradiance profiles measured during several Sodankylä upper-air flights from the surface to the lower stratosphere, which reveal the propagation of downward and upward shortwave and longwave radiation through cloud-free and cloudy atmospheres. By comparing longwave radiation profiles of different flights, the measurements show how variations in temperature and relative humidity change longwave radiative absorption and emission, and by this visualize and demonstrate radiative forcing and a changing greenhouse effect by water vapor and clouds in the Earth's atmosphere.

2 Atmospheric radiation profile measurements

The radiation profile measurements in 2011 (Philipona et al., 2012) showed promising results and led to further development of the instrumentation. The combination of an upward pyrgeometer and a downward pyranometer resulted in a much lighter and more compact instrument, in which all body and dome temperatures are measured at the inside walls of the instrument. Two such instruments, one mounted upside down, were built into the wings of the return glider radiosonde, which allows measuring the shortwave and longwave, upward and downward radiation components during the ascent, when the RGR is lifted in horizontal position 50 m below the weather balloon (Kräuchi and Philipona, 2016). During the uplift the RGR randomly rotates, which compensates for possible misalignments of its horizontal position. After release from the balloon between 20 and 30 km the RGR flies the instruments back to a predetermined location. The four radiometers are pre-calibrated by field comparisons to radiation standards, and the overall measurement uncertainty is $\pm 4\,\mathrm{W\,m^{-2}}$ for the longwave (Philipona et al., 2001) and $\pm 25\,\mathrm{W\,m^{-2}}$ for the shortwave radiometers (Kratzenberg et al., 2006). Irradiance differences observed between individual flights show considerably smaller uncertainties.

Fig. 1 shows the downward (positive) and upward (negative) irradiances of shortwave and longwave radiation measured during four daytime flights to about 20 km altitude. Temperature (T) and relative humidity (RH) are also shown. Flights 1 and 3 (left graphs) were under cloud-free conditions, while flights 2 and 4 (right graphs) had stratocumulus cloud layers below 3.5 km altitude, with 100 % relative humidity inside the cloud layers. Details on the four flights are shown in Table 1.

Incoming solar radiation is shown to be partly absorbed and reflected in the atmosphere, and under cloud-free skies shortwave downward radiation (SDR) and shortwave upward radiation (SUR) (bluish colors) are lowest at the surface. Shortwave net radiation (SNR) is the difference between SDR and SUR. The albedo, the fraction of incident radiation reflected by the surface, (−SUR/SDR at the surface) is on the order of 15 %, but due to reflection of incident solar radiation in the atmosphere it increases to >25 % at 20 km altitude. Clouds strongly reflect solar radiation and SDR is lowest at the lower edge of the cloud. The increase of solar radiation towards the ground surface below the cloud in flight 2 shows that the cloud thickness was not constant over large areas. SUR strongly increases through the cloud layer and shows largest values at the top of the cloud with albedo values of up to 75 %. Above this, the albedo decreases with altitude to about 50 % at 20 km with SUR decreasing more than SDR increases. Shortwave radiation of course strongly varies with the time of day, as shown between flight 1 with highest and flight 3 with lowest solar elevation angle.

Longwave radiation profiles (reddish colors) are more similar over the four flights. Longwave upward radiation (LUR) at the surface strongly depends on the surface skin temperature, which is higher for the noontime flight 1 than the early morning flight 3. In flights 2 and 4 LUR is absorbed inside cloud layers, which clearly re-

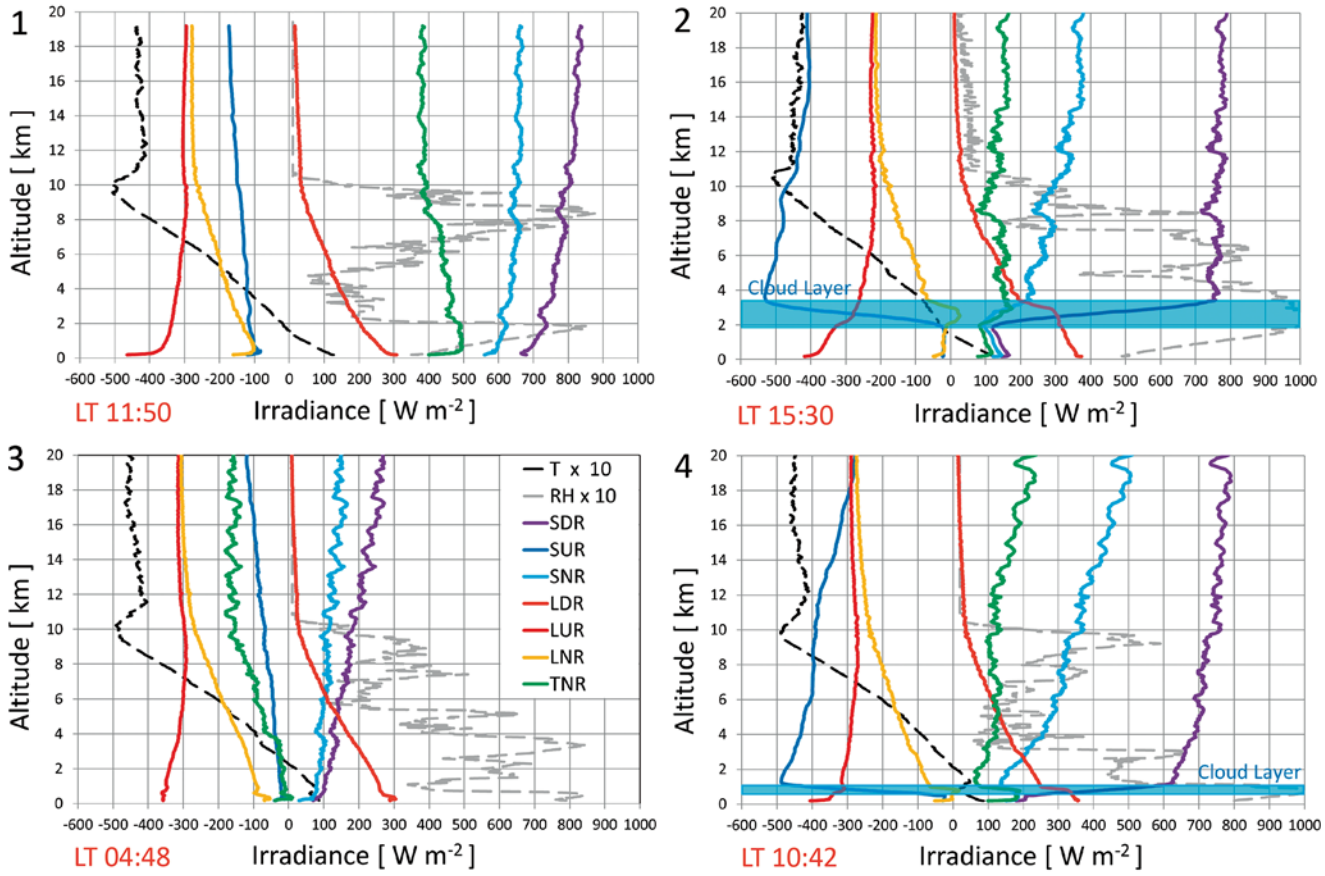

Figure 1: Atmospheric temperature, humidity and radiation profiles. Data are shown for cloud-free flights (flights 1 and 3 left) and flights with cloud layers (flights 2 and 4 right). Temperature (T) and humidity (RH) are given in [°C] and [%], respectively (divide horizontal scale by 10). Downward irradiances (SDR) and (LDR) are positive, and upward irradiances (SUR) and (LUR) negative. Shortwave net (SNR) is positive and longwave net (LNR) negative. The total net radiation (TNR) can be positive or negative. The local start time (LT) is shown below the graphs.

Table 1: a) Flight- and RGR registration number. Date, time at start, top and landing. Altitude at start and top. b) Flight numbers and surface values for pressure, temperature, relative humidity, and wind velocity and direction. Integrated water vapor and solar elevation angle at start and top.

a)

Flight Nr	RGR-Nr	Date	Time_Start [LT]	Time_Top [LT]	Time_Land [LT]	Alt_Start [m]	Alt_Top [m]
1	RGR9985	30.06.2015	11:50:02	12:54:13	13:44:16	176	19191
2	RGR9984	06.07.2015	15:30:34	16:21:13	17:27:00	176	19980
3	RGR9985	10.07.2015	04:48:01	06:17:37	07:05:20	176	23985
4	RGR9985	10.07.2015	10:42:14	11:49:58	12:25:40	176	24001

b)

Flight Nr	P [hPa]	T [°C]	RH [%]	W_vel [m/s]	W_dir [°]	IWV [mm]	SE_Start [°]	SE_Top [°]
1	995.7	13.0	29	1.4	357	15.5	45.63	45.47
2	993.2	13.3	48	1.7	228	18.7	36.51	32.08
3	985.2	8.2	79	1.8	17	15.0	12.26	20.29
4	987.1	8.3	81	2.9	36	13.3	42.42	44.69

duces emission to space. Clouds also strongly emit longwave downward radiation (LDR), which increases LDR below clouds compared to cloud-free conditions. Above the cloud altitude LDR is similar for all four flights, but in the troposphere LDR is highest in flight 2 and likely related to strong LUR absorption. At 20 km LDR is between 10 and 20 W m^{-2} and composed of terrestrial longwave emission, and of a small direct solar infrared component (Philipona et al., 2012). LDR in the lower stratosphere is slightly larger in flight 1 and 4 because the balloons were launched closer to noon time (see Table 1).

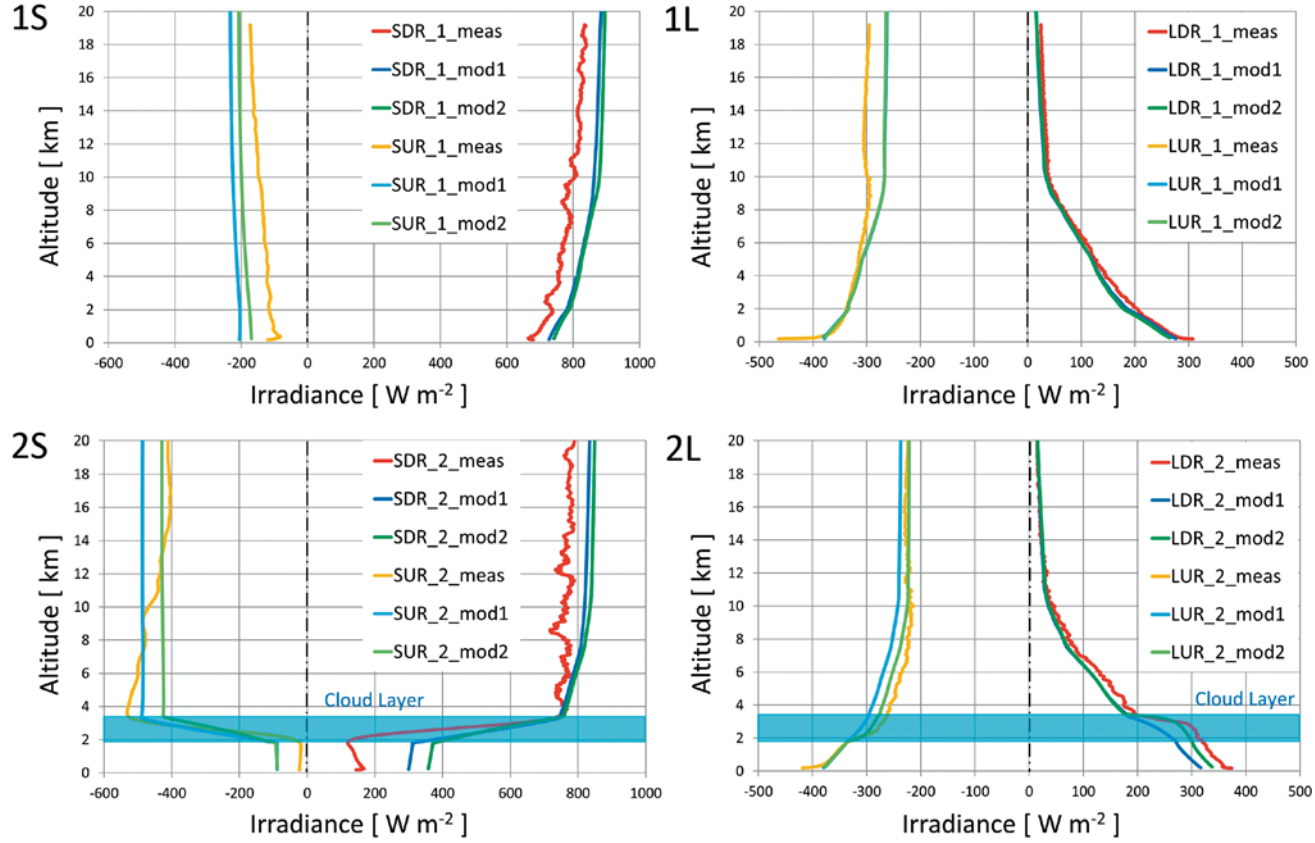

Figure 2: Measured versus modeled atmospheric radiation profiles. Measured shortwave profiles (SDR) and (SUR) are compared to model 1 and model 2 of flight 1 in graph 1S and of flight 2 in graph 2S (left). Longwave radiation profiles (LDR) and (LUR) of the two flights are compared to model calculations in graph 1L and graph 2L (right). Under cloud free conditions calculated longwave radiation profiles are exactly the same for both models (graph 1L).

Longwave net radiation (LNR) (orange) is always negative (upward) except inside of cloud layers. As LDR decreases towards higher altitude LNR becomes more negative and finally reaches the value of LUR at very high altitude, except for the small direct solar infrared component during daytime measurements. The overall total net radiation (TNR) (green) is observed to be positive in three flights and largest in flight 1, which is closest to solar noon and under cloud-free conditions. Negative TNR values have been observed during the cloud-free flight 3 with low solar elevation angle. Nighttime TNR is always negative except inside of clouds (Philipona et al., 2012).

3 Measured versus calculated radiation

Radiative transfer model calculations of shortwave and longwave irradiance profiles have been performed by two groups individually, using MstrnX (Sekiguchi and Nakajima, 2008) (model 1) and Streamer (Key and Schweiger, 1998) (model 2). In both models the same available atmospheric data measured during the Sodankylä flights were used. Fig. 2 shows comparisons of measured and calculated shortwave profiles of the cloud-free flight 1 and the cloudy flight 2 (1S and 2S, left graphs), and of longwave radiation profiles of the same flights (1L and 2L, right graphs).

Measured and calculated shortwave radiation profiles (graph 1S and 2S) show differences of up to 50 W m^{-2} on SDR and up to almost 100 W m^{-2} on SUR. Calculated shortwave downward radiation shows differences of up to 30 W m^{-2} between the two models and is generally larger than the measured values. Under cloudy conditions (graph 2S) model 1 shows better agreement with the measurements below the cloud. Shortwave upward radiation of model 2 is slightly closer to the measurements primarily in the lower stratosphere, whereas in the cloud and in the troposphere above the cloud model 1 shows better agreement with the measurements.

Longwave radiation profiles show better agreement between calculations and measurements. Under cloud-free conditions (graph 1L) models 1 and 2 slightly underestimate LDR measurements as previously observed (Wild et al., 2001). LUR shows good agreement in the lower troposphere, except for the near surface. However, both models underestimate the emission into space. With the cloud layer model calculations still slightly underestimate LDR measurements, but overall the Streamer model 2 shows considerably better agreement with the measurements than the MstrnX model 1.

Differences between the two model calculations are small under cloud free situations, except for SUR which shows differences of up to 30 W m^{-2}. With clouds, the differences for shortwave and longwave radiation reach up to 60 W m^{-2}, even though both models used the same input data. However, comparisons between measurements and model calculations show considerably larger differences, but better agreement is found for terrestrial than for solar radiation. Part of the reason for the large discrepancies may be the fact, that the upper-air measurements were made over large areas (up to 50 km radius) with inhomogeneous ground surfaces, forests, open land and lakes. The input parameters for the models, which are from the balloon launch station, are therefore not necessarily realistic for the entire flight. Also, vertical profiles of pressure, temperature and water vapor are from the operational radiosonde launched at the Sodankyla site the same day, and ozone profiles are available once per week. This means, that the profile data used in the model calculations are not necessarily measured at the exact same time as the radiation profiles. Furthermore, cloud layers were not homogeneous over the investigated area and the time of flight. At the surface, differences may be related to the partly forested terrain environment at the Sodankylä aerological station, where direct solar absorption leads to considerably higher surface skin temperatures in forest free areas than the air temperature measured at the 2-meter level (see chapter 4). All these different circumstances are in part responsible for the observed differences between the model calculated and the measured irradiances.

4 Longwave radiative forcing and the greenhouse effect

Effects of changing temperature, relative humidity and cloud layers on upward and downward longwave radiation in the troposphere are further investigated by comparing temperature, relative humidity and longwave radiation profiles of different flights. Fig. 3 shows two graphs with comparisons of two flights each, under cloud-free or cloudy conditions. Fig. 3 also shows theoretical values of the upward and downward longwave radiation calculated with the Stefan-Boltzmann law: LWR = $\varepsilon_{\text{eff}}\sigma T^4$. For these theoretical calculations the effective emissivity ε_{eff} is set to 1 at the surface and for all altitudes for the upward and the downward longwave radiation. σ is the Stefan Boltzmann constant [5.67×10^{-8} W m^{-2} K^{-4}] and T is the respective temperature in Kelvin [K].

Fig. 3a compares the two cloud-free flights 1 and 3. The temperature 2 m above ground is higher in the noon time flight 1 than in the early morning flight 3. At an altitude of 800 m the temperature T_3 shows an inversion, and further up it is roughly 3 °C higher than the temperature T_1. From 2 to 5.5 km, the relative humidity RH_1 shows a distinct dry layer compared to RH_3, but further up from 5.5 to 10 km RH_1 exceeds RH_3. The strong LUR_1 surface emission of −464 W m^{-2} corresponds, according to the Stephan-Boltzmann law, to a surface skin temperature of 28.6 °C, which due to solar radiation absorption is much higher than the measured 2-meter air temperature of 13 °C. In contrast, in the early morning flight LUR_3 with −358 W m^{-2} emission, the surface skin temperature is only 0.9 °C higher than the 2-meter air temperature. LUR_1 strongly decreases and is shown to follow Stefan-Boltzmann emission in the first 100 to 800 m above ground with an effective emissivity of roughly 1. However, above 800 m and with decreasing air pressure at higher altitudes longwave upward radiation more freely propagates and does not follow Stefan Boltzmann emission at local air temperature. Between 2 and 5.5 km higher relative humidity RH_3 absorbs LUR_3, such that at 3.5 and 5.5 km altitude LUR_3 is lower than LUR_1 despite its higher temperature. LUR_1 and LUR_3 then show similar values and just above the tropopause both slightly increase due to the rising temperature inside a prominent ozone layer (see Fig. 4).

Longwave downward radiation LDR_1 above the tropopause is larger than LDR_3 because flight 1 was launched around noon time and therefore has a higher direct solar component. Due to the higher temperature T_3 below the tropopause LDR_3 becomes slightly larger than LDR_1. Below 5.5 km the slopes of LDR_1 and LDR_3 both change because RH_1 decreases and RH_3 increases. The increase of LDR_3 with RH_3 is consistent with the enhanced LUR_3 absorption at these altitudes mentioned above, and shows that increased humidity values lead to enhanced LUR absorption and also to enhanced LDR emission. This relation between longwave radiation absorption/emission and humidity experimentally visualizes a changing water vapor greenhouse effect. At the surface LDR_1 is slightly larger than LDR_3 because the temperature T_1 is higher.

Fig. 3b compares flights 1 and 2 with similar temperature in the lower troposphere. The relative humidity RH_2 reaches 100 % inside the cloud layer and stays high up to 7.5 km altitude. With lower surface skin temperature below the cloud, longwave emission at the surface is smaller in flight 2, otherwise LUR of both flights are similar with similar temperature and relative humidity. Passing through the cloud LUR_2 loses 65 W m^{-2}, and at cloud top the emission of −261 W m^{-2} and the measured air temperature of −8.2 °C corresponds to an effective emissivity of about 0.95. From here to 7.5 km altitude LUR_2 is more strongly absorbed due to a higher relative humidity even though temperature is slightly higher. This high LUR_2 absorption above the cloud results in a strong LDR_2 emission at these altitudes, which again demonstrates increased greenhouse emission due to the higher water vapor amount. Above 7.5 km altitude LDR_2 remains higher, due to the higher temperature T_2. This only switches above the tropopause, where T_1 shows more rapid warming in the ozone layer. In the upper part of the cloud LDR_2

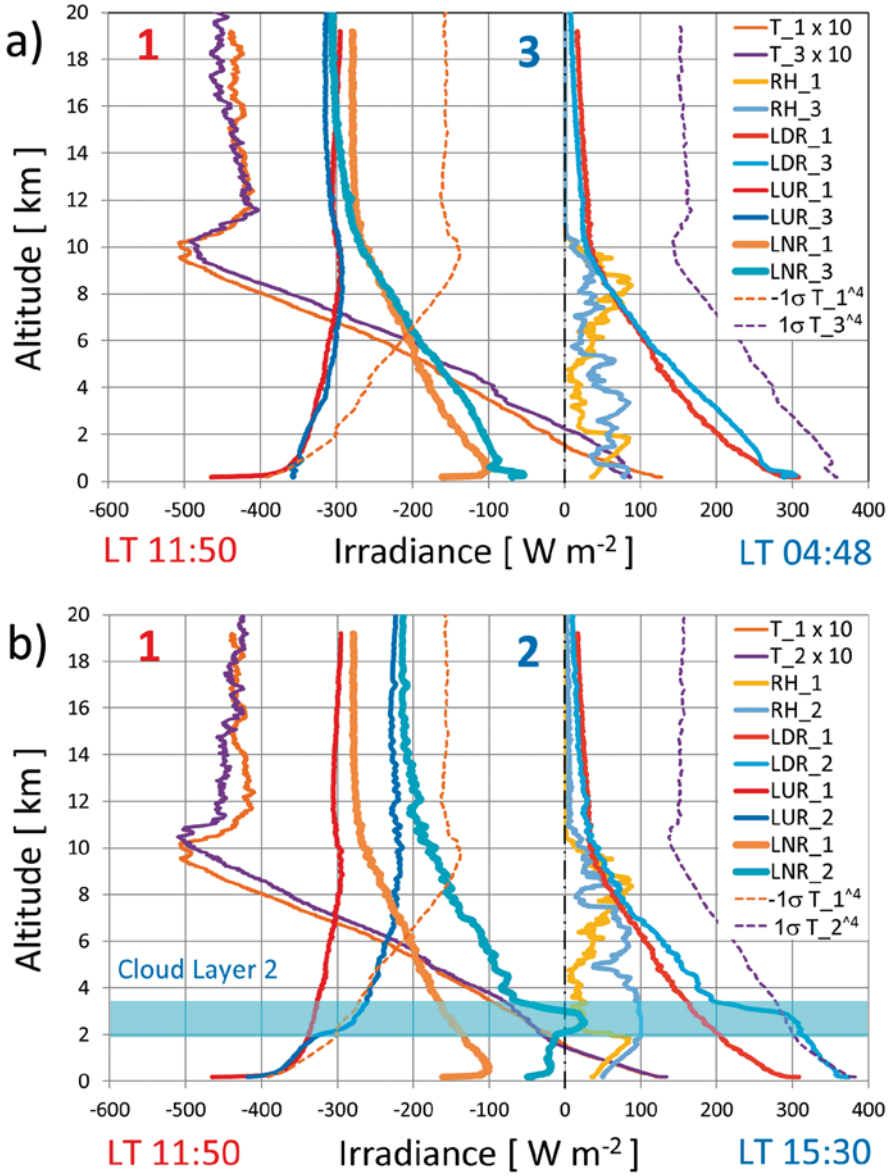

Figure 3: Comparisons of temperature, humidity and longwave radiation of two flights. (a) flights 1 (clear sky) and flight 3 (clear sky). (b) flights 1 (clear sky) and flight 2 (cloudy sky). Temperature (T) in [°C] (divide horizontal scale by 10), relative humidity (RH) in [%]. Longwave downward (LDR) radiation is positive (incoming) and longwave upward (LUR) radiation as well as longwave net (LNR) radiation are negative (outgoing). Theoretical values of the upward and downward longwave radiation calculated with the Stephan-Boltzmann law and a fixed emissivity of 1 are shown for one flight each. The local start time (LT) is below the graphs.

increases by 110 W m^{-2}, which is larger than the LUR_2 absorption in the cloud. This is consistent with the positive LNR shown in Fig. 1 flight 2. Below the cloud LDR_2 is smaller than LUR_2 and follows more or less the Stefan-Boltzmann emission according to the measured temperature and an effective emissivity close to 1.

Radiative forcing, as introduced in the introduction, results from an imbalance on incoming and outgoing energy in the Earth-atmosphere system either through solar or terrestrial radiation. With rising anthropogenic greenhouse gases outgoing longwave radiation is reduced through enhanced absorption of terrestrial longwave radiation, which results in radiative forcing and an enhanced greenhouse effect of planet Earth. The comparisons of radiation profiles of different flights in Fig. 3, demonstrate radiative forcing. Fig. 3a shows larger amounts of water vapor in flight 3 than 1 in the lower half of the troposphere, which results in reduced longwave net radiation LNR_3 compared to LNR_1, even though the temperature T_3 is higher than T_1. However, in the upper part of the troposphere the considerably larger amount of water vapor RH_1 compared to RH_3 strongly reduces the outgoing longwave net radiation LNR_1 compared to LNR_3. An even larger reduction of outgoing longwave net radiation is due to clouds as shown in the comparison in Fig. 3b, which shows clearly reduced longwave net radiation LNR_2 due to the cloud layer in flight 2 compared to the cloud-free LNR_1 throughout the atmosphere. Both comparisons demonstrate radiative forcing and a change of the

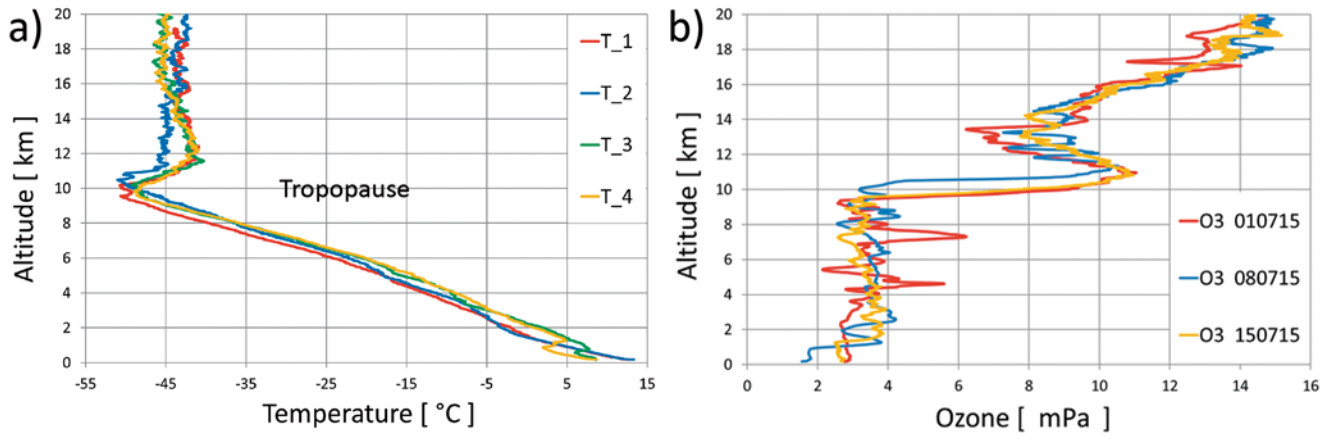

Figure 4: Temperature reversal due to an ozone layer above the tropopause. a) Temperature profiles (T) of the four flights to 20 km altitude. b) Ozone vertical profiles (O3) measured above Sodankylä on 01., 08. and 15. July 2015.

greenhouse effect due to water vapor and clouds, and evidence strong longwave warming to be expected from humid Cirrus clouds.

5 Discussion and conclusions

Measured shortwave and longwave radiation profiles reveal the radiative effects of temperature, water vapor, ozone and clouds on downward and upward radiation in the atmosphere, as well as albedo effects at the ground surface. Aerosols and other atmospheric gases also affect solar and terrestrial radiation but their changes between the four flights were small and therefore here not detectable. Simultaneous measurements of temperature, relative humidity, ozone and radiation profiles reveal the effects of temperature, water vapor and ozone on irradiances. Comparisons of profiles of different flights on the other hand, allow clear determinations of the effects of enhanced absorption/emission of upward/downward longwave radiation, respectively, caused by variations in temperature, water vapor and clouds.

Radiative transfer model calculations show similar profile aspects as the measured shortwave and longwave irradiance profiles, but measured profiles show considerably more details of the local absorption and emission. Also, the discrepancies between the measured and the calculated profiles are quite large. The reason for the differences between measurements and model calculations are possibly due to the large inhomogeneities on the ground surface and on the cloud layer over which the measurements were made, and the fact that the input for the model calculations is from the balloon launch station and from the operational radiosonde. However, the comparison between radiation measurements and model calculations also show, that input parameters for the models are very crucial to reproduce the full reality with model calculations.

Solar absorption by water vapor in the troposphere is clearly observable in shortwave radiation profiles. Under cloud-free skies, albedo is therefore lowest at the surface and increases with altitude. Reflection of shortwave radiation from clouds is somewhat spectrally dependent and also depends on cloud microphysics. Cloud reflection is crucial with respect to shortwave albedo and the overall solar reflection back into space. Shortwave albedo is highest at the cloud top and decreases towards higher altitude. Strong reflection is also observed inside of clouds, and at the bottom of cloud layers shortwave radiation is comparable to irradiances at the ground surface.

Surface emission of terrestrial longwave radiation is related to the ground surface skin temperature, which depends on solar absorption by the surface. But, surface emission is strongly attenuated and controlled by air temperature and water vapor in the first 100 to 800 meter above ground and corresponds to Stefan-Boltzmann emission with an effective emissivity close to 1. However, with decreasing pressure at higher altitudes the longwave upward radiation more freely propagates and no longer follows Stefan-Boltzmann emission, but rather depends on the boundary layer and surface temperature. Above the tropopause a temperature inversion due to an ozone layer slightly increased upward longwave radiation in all Sodankylä flights. Clouds strongly absorb upward longwave radiation primarily in the lower part of the cloud. At the cloud top longwave emission corresponds to Stefan-Boltzmann emission with an effective emissivity of about 0.95. Longwave downward radiation strongly increases in the upper part of cloud layers, which leads to a positive (downward) longwave net radiation. Below the clouds it follows the Stefan-Boltzmann law and an effective emissivity close to 1.

Most interesting however, are the observed variations of terrestrial longwave absorption and emission due to changing temperature and varying water vapor amounts. Flight comparisons show that larger amounts of water vapor always enhance longwave upward absorption and longwave downward emission. The observed changes of water vapor and the respective changes of longwave upward and downward radiation show the warming effect of increasing greenhouse gases, and experimentally

demonstrate radiative forcing and an increase of the water vapor greenhouse effect in the Earth's atmosphere. Radiative forcing and an increased greenhouse effect are also clearly shown by longwave net radiation profiles in cloudy compared to cloud-free atmospheres.

Acknowledgments, samples, and data

The authors have no competing interests, or other interests that might be perceived to influence the interpretation of the article.

Technical information and details on the different flights are available in a previously published paper on the return glider radiosonde (Kräuchi and Philipona, 2016).

The authors would like to thank the personnel at the Finnish Meteorological Institute (FMI) Sodankylä site for the support to realize the flight campaign. We are also very thankful to the Air Navigation Services Finland (ANS Finland), which allowed us to perform test flights and first scientific measurements of upper-air radiation profiles with our drone the Return Glider Radiosonde at the Space and Earth Observation Center in Sodankylä.

References

Asano, S., Y. Yoshida, Y. Miyake, K. Nakamura, 2004: Development of a radiometer-sonde for simultaneously measuring the downward and upward broadband fluxes of shortwave and longwave radiation. – J. Meteor. Soc. Jpn. **82**, 623–637, DOI:10.2151/jmsj.2004.623.

Eyring, V., N.R.P. Harris, M. Rex, T.G. Shepherd, D.W. Fahey, G.T. Amanatidis, J. Austin, M.P. Chipperfield, M. Dameris, P.M. De, F. Forster, A. Gettelman, H.F. Graf, T. Nagashima, P.A. Newman, S. Pawson, M.J. Prather, J.A. Pyle, R.J. Salawitch, B.D. Santer, D.W. Waugh, 2005: A Strategy for process-oriented validation of coupled chemistry–climate models. – Bull. Amer. Meteor. Soc. **86**, 1117–1133, DOI:10.1175/BAMS-86-8-1117.

Fröhlich, C., 1991: History of solar radiometry and the world radiometric reference. – Metrologia **28**, 111–115.

Fröhlich, C., J.L. Lean, 2004: Solar radiative output and its variability: Evidence and mechanisms. – Astron. Astrophys. Rev. **12**, 273–320.

Foukal, P., C. Fröhlich, H. Spruit, T.M.L. Wigley, 2006: Variations in solar luminosity and their effect on the Earth's climate. – Nature **443**, 161–166, DOI:10.1038/nature05072.

Global Climate Observing System (GCOS), 2007: Rep. GCOS-112. – World Meteor. Organ., Geneva, Switzerland, 55 pp.

Guan, H., B. Schmid, A. Bucholtz, R. Bergstrom, 2010: Sensitivity of shortwave radiative flux density, forcing, and heating rate to the aerosol vertical profile. – J. Geophys. Res. **115**, D06209, DOI:10.1029/2009JD012907.

Hansen, J., L. Nazarenko, R. Ruedy, M. Sato, J, Willis, A. Del Genio, D. Koch et al., 2005: Earth's energy imbalance: Confirmation and implications. – Science **308**, 1431–1435, DOI:10.1126/science.1110252.

Held, I.M., B.J. Soden, 2000: Water vapor feedback and global warming. – Ann. Rev. Energy Env. **25**, 441–475, DOI: 10.1146/annurev.energy.25.1.441.

Key, J., A.J. Schweiger, 1998: Tools for atmospheric radiative transfer: Streamer and FluxNet. – Computers Geosci. **24**, 443–451.

Kopp, G., J.L. Lean, 2011: A new, lower value of total solar irradiance: Evidence and climate significance. – Geophys. Res. Lett. **38**, L01706, DOI:10.1029/2010GL045777.

Kratzenberg, M.G., H.G. Beyer, S. Colle, A. Albertazzi, 2006: Uncertainty calculations in pyranometer measurements and applications. – Proceedings of ISEC2006, ASME International Solar Energy Conference, July 8–13, 2006, Denver, CO.

Kräuchi, A., R. Philipona, 2016: Return glider radiosonde for in situ upper-air research measurements. – Atmos. Meas. Tech. **9**, 2535–2544, DOI:10.5194/amt-9-2535-2016.

Kräuchi, A., R. Philipona, G. Romanens, D.F. Hurst, E.G. Hall, A.F. Jordan, 2016: Controlled weather balloon ascents and descents for atmospheric research and climate monitoring. – Atmos. Meas. Tech. **9**, 929–938, DOI:10.5194/amt-9-929-2016.

Ohring, G., P. Clapp, 1980: The Effect of changes in cloud amount on the net radiation at the top of the Atmosphere. – J. Atmos. Sci. **37**, 447–454, DOI:10.1175/1520-0469(1980)037<0447:TEOCIC>2.0.CO;2.

Paltridge, G.W., S.L. Sargent, 1971: Solar and thermal measurements to 32 km at low solar elevations. – J. Atmos. Sci. **28**, 242–253, DOI:10.1175/1520-0469(1971)028<0242:SATRMT>2.0.CO;2.

Philipona, R., E.G. Dutton, T. Stoffel, J. Michalsky, I. Reda, A. Stifter, P. Wendung, N. Wood, S.A. Clough, E.J. Mlawer, G. Anderson, H.E. Revercomb, T.R. Shippert, 2001: Atmospheric longwave irradiance uncertainty: Pyrgeometers compared to an absolute sky-scanning radiometer, atmospheric emitted radiance interferometer, and radiative transfer model calculations. – J. Geophys. Res. **106**, 28129–28141, DOI:10.1029/2000JD000196.

Philipona, R., B. Dürr, C. Marty, A. Ohmura, M. Wild, 2004: Radiative forcing – measured at Earth's surface – corroborate the increasing greenhouse effect. – Geophys. Res. Lett. **31**, L03202, DOI:10.1029/2003GL018765.

Philipona, R., A. Kräuchi, E. Brocard, 2012: Solar and thermal radiation profiles and radiative forcing measured through the atmosphere. – Geophys. Res. Lett. **39**, L13806, DOI: 10.1029/2012GL052087.

Philipona, R., C. Mears, M. Fujiwara, P. Jeannet, P. Thorne, G. Bodeker, L. Haimberger, M. Hervo, Ch. Popp, G. Romanens, W. Steinbrecht, R. Stübi, R. van Malderen, 2018: Radiosondes show that after decades of cooling, the lower stratosphere is now warming. – J. Geophys. Res. **123**, DOI:10.1029/2018JD028901.

Ramanathan, V., R.D. Cess, E.F. Harrison, P. Minnis, B.R. Barkstrom, E. Ahmad, D. Hartmann, 1989: Cloud-radiative forcing and climate: Results from the Earth radiation budget experiment. – Science **243**, 57–63, DOI:10.1126/science.243.4887.57.

Randel, W.J., F. Wu, H. Vömel, G. E Nedoluha, P. Forster, 2006: Decreases in stratospheric water vapor after 2001: Links to changes in the tropical tropopause and the Brewer-Dobson circulation. – J. Geophys. Res. **111**, D12312, DOI:10.1029/2005JD006744.

Raschke, E., T.H. Vonder Haar, W.R. Bandeen, M. Pasternak, 1973: The annual radiation balance of the Earth-Atmosphere system during 1969–70 from Nimbus 3 measurements, – J. Atmos. Sci. **30**, 341–364, DOI:10.1175/1520-0469(1973)030<0341:TARBOT>2.0.CO;2.

Seidel, D.J., F.H. Berger, H.J. Diamond, J. Dykema, D. Goodrich et al., 2009: Reference upper-air observations for climate: Rationale, progress, and plans. – Bull. Amer. Meteor. Soc. **90**, 361–369, DOI:10.1175/2008BAMS2540.1.

Sekiguchi, M., T. Nakajima, 2008: A k-distribution-based radiation code and its computational optimization for an atmospheric general circulation model. – J. Quant. Spectroscopy Radiative Transfer, DOI:10.1016/j.jqsrt.2008.07.013.

Solomon, S., K.H. Rosenlof, R.W. Portmann, J.S. Daniel, S.M. Davis, T.J. Sanford, G.K. Plattner, 2010: Contributions of stratospheric water vapor to decadal changes in the rate of global warming. – Science **327**, 1219–1223, DOI: 10.1126/science.1182488.

Suomi, V.E., D.O. Staley, P.M. Kuhn, 1958: A direct measurement of infra-red radiation divergence to 160 millibars. – Quart. J. Roy. Meteor. Soc. **84**, 134–141, DOI:10.1002/qj.49708436006.

Thorne, P.W., D.E. Parker, J.R. Christy, C. Mears, 2005: Uncertainties in climate trends: Lessons from upper-air temperature records. – Bull. Amer. Meteor. Soc. **86**, 1437–1442, DOI:10.1175/BAMS-86-10-1437.

Trenberth, K.E., J.T. Fasullo, J. Kiehl, 2009: Earth's Global Energy Budget. – Bull. Amer. Meteor. Soc. **90**, 311–324, DOI: 10.1175/2008BAMS2634.1.

Watanabe, S., T. Hajima, K. Sudo, T. Nagashima, T. Takemura, H. Okajima et al., 2011: MIROC-ESM 2010: model description and basic results of CMIP5-20c3m experiments. – Geosci. Model Dev. **4**, 845–872, DOI:10.5194/gmd-4-845-2011.

Wendisch, M., A. Keil, 1999: Discrepancies between measured and modeled solar and UV radiation within polluted boundary layer clouds. – J. Geophys. Res. **104**, 27373–27385.

Wendisch, M., B. Mayer, 2003: Vertical distribution of spectral solar irradiance in the cloudless sky – A case study. – Geophys. Res. Lett. **30**, 1183–1186, DOI:10.1029/2002GL016529.

Wendisch, M., S. Mertes, A. Ruggaber, T. Nakajima, 1996: Vertical profiles of aerosol and radiation and the influence of a temperature inversion: Measurements and radiative transfer calculations. – J. Appl. Meteor. **35**, 1703–1715.

Wendling, P., A. Stifter, B. Mayer, M. Fiebig, C. Kiemle, H. Flentje, M. Wendisch, W. Armbruster, U. Leiterer, W. von Hoyningen-Huene, A. Petzold, 2002: Aerosol-radiation interaction in the cloudless atmosphere during LACE 98, 2, Aerosol-induced solar irradiance changes determined from airborne pyranometer measurements and calculations. – J. Geophys. Res. **107**, 8131, DOI:10.1029/2000JD000288.

Wild, M., A. Ohmura, H. Gilgen, J.J. Morcrette, A. Slingo, 2001: Downward longwave radiation in General Circulation Models. – J. Climate **14**, 3227–3239.

Wild, M., J. Grieser, C. Schär, 2008: Combined surface solar brightening and increasing greenhouse effect support recent intensification of the global land-based hydrological cycle. – Geophys. Res. Lett. **35**, L17706, DOI:10.1029/2008GL034842.

Willson, R.C., 1997: Total solar irradiance trend during solar cycles 21 and 22. – Science **277**, 1963–1965.

Yamamoto, A., T. Yamanouchi, M. Wada, 1995: Effective emissivity of clouds from radiometersonde measurements at Syova station. Antarctica. Proc. NIPR Symp. – Polar Meteor. Glaciol. **9**, 133–145.